Eur. Phys. J. D **42**, 243–251 (2007)
DOI: 10.1140/epjd/e2007-00017-9

THE EUROPEAN PHYSICAL JOURNAL D

Formation of silver nanoclusters in transparent polyimides by Ag-K ion-exchange process

S. Carturan[1,a], A. Quaranta[2], M. Bonafini[3,b], A. Vomiero[3,c], G. Maggioni[1], G. Mattei[4], C. de Julián Fernández[4], M. Bersani[4], P. Mazzoldi[4], and G. Della Mea[2]

[1] University of Padova, c/o Istituto Nazionale di Fisica Nucleare, Laboratori Nazionali di Legnaro, Viale dell'Università 2, 35020 Legnaro, Padova, Italy
[2] Department of Materials Engineering and Industrial Technologies, University of Trento, Trento, Italy
[3] Istituto Nazionale di Fisica Nucleare, Laboratori Nazionali di Legnaro, Viale dell'Università 2, 35020 Legnaro, Padova, Italy
[4] Department of Physics, University of Padova, Via Marzolo 8, 35131 Padova, Italy

Received 5 October 2006 / Received in final form 13 December 2006
Published online 31 January 2007 –

Abstract. Silver nanoclusters embedded in two transparent fluorinated polyimides, 4,4'-hexafluoroisopropylidene diphthalic anhydride — 2,3,5,6-tetramethyl paraphenylene diamine (6FDA-DAD) and 3,3',4,4' — biphenyltetracarboxylic acid dianhydride — 1,1-bis(4-aminophenyl)-1-phenyl-2,2,2-trifluoroethane (BPDA-3F), have been produced by surface modification with KOH aqueous solution followed by K-assisted Ag doping and thermal reduction in hydrogen atmosphere. The reaction rate of the nucleophilic hydrolysis in KOH, studied by Fourier transform infrared spectroscopy (FT-IR) and Rutherford backscattering spectrometry (RBS), depends on the polyimide chemical structure. After ion-exchange in $AgNO_3$ solution and subsequent annealing, the polyimide structure recovery was monitored by FT-IR whereas the characteristic surface plasmon absorption band of silver nanoparticles was evidenced by optical absorption measurements. The structure of silver nanoclusters as related to size and size distribution in the different polyimide matrices was thoroughly investigated by Transmission electron microscopy (TEM) and X-ray diffraction (XRD). The collected data evidenced a uniform distribution of Ag clusters of nanometric size after thermal treatment at 300 °C in both polyimides. For the same ion-exchange treatment parameters and annealing temperature, XRD analyses evidenced the presence of crystallites with similar sizes.

PACS. 71.20.Rv Polymers and organic compounds – 82.30.Nr Association, addition, insertion, cluster formation – 36.40.Vz Optical properties of clusters

1 Introduction

Nowadays a number of investigations are focused on the production of nanocomposite materials made up of metal nanoclusters embedded in organic matrices, owing to their unusual optical, electronic, magnetic and chemical properties [1,2]. In fact, the incorporation of metal particles in polymeric hosts allows their stabilization and prevents agglomeration, thus facilitating the fabrication into useful catalytic, optical and electronic devices. The optical properties of noble metal nanoparticles (Cu, Au, Ag) are related to a typical absorption peak in the UV-VIS range [3], known as surface plasmon resonance (SPR) peak, whose intensity, position and band-width are affected by the size, size distribution and shape of the nanoparticles. Furthermore, since the SPR peak features are strongly correlated to the physico-chemical nature of the host medium [4,5], the possibility to exploit the optical properties of this kind of nanocomposites in the optical sensing field has received increasing attention [6,7]. Metal-polymer nanocomposites have been usually prepared by mixing metal particles with polymer solutions [8], by vacuum co-deposition procedures [9,10], by metal precursor doping and decomposition [11–14], and by ion implantation [15,16]. Recent papers investigated the synthesis of metal clusters into commercially available polyimides obtained by ion-exchange technique followed by annealing in reducing atmosphere [17–20]. This method relies on a surface treatment of the bare polyimide films in KOH to produce a surface-modified polyimide layer (potassium polyamate) with ion-exchange capability. Thereafter, metal ions are introduced through ion-exchange with the bound potassium ions. By a subsequent annealing in reducing

[a] e-mail: carturan@lnl.infn.it
[b] *Present address*: Spinlab1 srl, Via Bellavitis 19, Bassano del Grappa, Vicenza, Italy.
[c] *Present address*: INFM Sensor Laboratory, Via Valotti 9, 25133 Brescia, Italy.

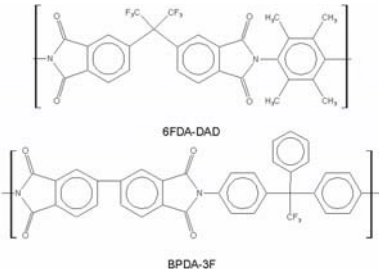

Fig. 1. Chemical structures of the 6FDA-DAD and BPDA-3F polyimides.

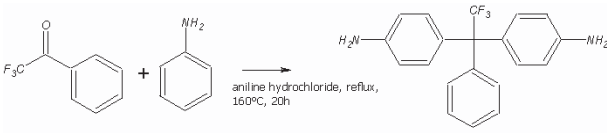

Fig. 2. Reaction scheme for the synthesis of the diamine 3F.

atmosphere, the re-imidization of the polyimide and the metal nanoparticle precipitation are promoted. Unfortunately, commercial aromatic polyimides, like Kapton® or Upilex®, are not optically transparent in the whole visible range. Therefore, the study of the optical properties of silver clusters, which are known to exhibit a peak in the range of 370−480 nm depending on the matrix and particle size, is precluded. Among the different polyimides, fluorinated polyimides exhibit improved optical transparency in the visible range with respect to commercial polyimides [21]. This feature makes them good candidates for the production of silver-polyimide nanocomposites in which the optical properties of silver nanoclusters are fully exploited. In this work, we report the preparation of silver nanoclusters into two transparent fluorinated polyimides by an ion-exchange technique, aiming at a deeper comprehension of the Ag-doping mechanism.

2 Experimental

2.1 Synthesis of the 6FDA-DAD and BPDA-3F polyimides

The starting polyimides were 4,4'-hexafluoroisopropylidene diphthalic anhydride — 2,3,5,6-tetramethyl paraphenylene diamine (6FDA-DAD) and 3,3',4,4' — biphenyltetracarboxylic acid dianhydride — 1,1-bis(4-aminophenyl)-1-phenyl-2,2,2-trifluoroethane (BPDA-3F), whose chemical structure is sketched in Figure 1.

All the reagents and the solvents used for the synthesis were purchased from Acros Chemicals and purified prior to use, apart from the diamine 3F, which was synthesized as described in Figure 2, according to the method proposed by Alston and Gratz [22].

The dianhydrides 6FDA and BPDA were sublimed under vacuum, whereas 2,3,5,6-tetramethyl-1,4-phenylenediamine (DAD) was purified by recrystallization from dichloromethane. The polyimides were synthesized by following the two-step classical

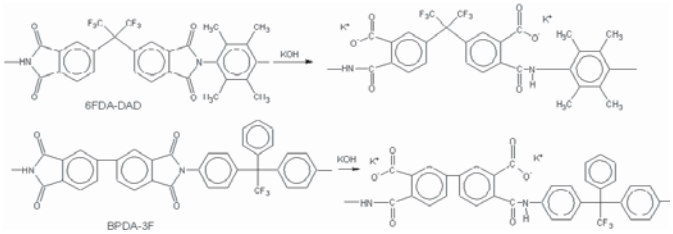

Fig. 3. Alkaline hydrolysis reaction scheme for 6FDA-DAD and BPDA-3F in KOH.

reaction scheme. The diamine was dissolved at room temperature in freshly distilled dimethylformamide under nitrogen flux. After a complete dissolution of the diamine an equimolar amount of dianhydride was added so as to obtain a solution 15% wt in solids which was stirred for 24 hours. The chemical imidization was obtained as follows. A solution of triethylamine and acetic anhydride (molar ratio 1:1) was added to the solution containing the polyamic acid, in such amount that the moles of triethylamine were fourfold the moles of each monomer. The resulting solution was stirred at 120 °C for 20 hours and then precipitated in methanol. The white polyimide powders were collected by filtration under reduced pressure, washed twice in water and twice in methanol and dried in air overnight and in vacuum at 200 °C for 15 hours.

2.2 Preparation of composite films

Self-supporting 30 μm thick films were obtained by the tape-casting technique, starting from the solution of each polyimide (10% wt. solids) in N-methylpyrrolidone. After drying in vacuum at 200 °C for 8 hours, the samples were immersed in KOH 5M for time intervals ranging from 1 min up to 20 min at 45 °C. Both polyimides react with KOH to give the salt potassium polyamate, as reported in Figure 3. Subsequently, the samples were thoroughly rinsed in deionized water and immersed in a solution of $AgNO_3$ 50 mM at 45 °C, thus undergoing the ion-exchange process between potassium and silver ions. The K^+-Ag^+ ion-exchange reached the nearly complete saturation within the first minutes of treatment in $AgNO_3$ aqueous solution. Anyway, the ion-exchange procedure was performed for time intervals two times longer with respect to the KOH treatment time, in order to assure the complete substitution of all the potassium ions within the modified layer. Thermal reduction of silver and particles aggregation were attained by annealing the samples in reducing atmosphere (H_2 12% - Ar) at temperatures lower or near the glass transition temperature (T_g) values (200 °C, 300 °C and 350 °C) for 30 min.

2.3 Analytical techniques

Fourier transform infrared spectroscopy (FTIR) in the mode of attenuated total reflectance (ATR) with a

standard ZnSe crystal was performed under vacuum at room temperature with a resolution of 4 cm^{-1} using a Jasco 660 Plus spectrometer.

Differential Scanning Calorimetry (DSC) was performed at a heating rate of 10 °C min^{-1} in N_2 (flow rate of 100 sccm) with a TA Instrument, while Thermogravimetric Analysis (TGA) was conducted in static air with a NETZSCH Simultaneous Thermal Analyzer STA 409.

UV-vis transmission and absorption spectra were recorded using a Jasco V530 spectrometer, at ambient temperature.

In order to study the nanostructural features of the composite films X-ray diffraction spectra were collected in the mode Grazing Incidence X-ray Diffraction (GIXRD). The measurements were carried out using a Panalytical X'Pert Pro MRD X-ray diffractometer working in Parallel Beam geometry and equipped with an X-ray tube emitting CuKα radiation (λ CuKα = 0.154186 nm). During the GIXRD measurements, the incident X-ray beam was fixed at an incidence angle of 0.5° or of 1° while the detector was moved along the goniometer circle in the 2θ range between 10° and 90°. Cross sectional transmission electron microscopy (TEM) was carried out at CNR-IMM Institute in Bologna with a field emission gun FEI TECNAI F20 (S)TEM microscope operating at 200 kV.

The K and Ag concentration and in-depth distribution were analysed by Rutherford backscattering spectrometry (RBS) using a 2.0 MeV $^4He^+$ beam (scattering angle θ = 160°) at the INFN-Laboratori Nazionali di Legnaro. A low current density (<7 nA/mm^2) was applied in order to avoid sample overheating. According to the stardard methodology of data analysis for the RBS technique, the experimental spectra were normalised to the total charge impinging on the sample and to the solid angle subtended by the detector. The backscattering data were analyzed using the commercial program RUMP [23].

3 Results and discussion

3.1 Optical and thermal properties of the bare polyimides

The optical transmission spectra of the 6FDA-DAD and BPDA-3F polyimides (thickness of 30 μm) and of some commercial polyimides foils (25 μm thick) are compared in Figure 4. Table 1 shows two parameters, which allow to better appreciate the different transparency between the tested polyimides: the transmission onset (cut-off wavelength) and the 80% transmission wavelength.

Both parameters of 6FDA-DAD and BPDA-3F polyimides are much lower with respect to the commercial ones, thus pointing out their particularly high transparency which allows to appreciate the absorption band related to the surface plasmon resonance of silver nanoclusters.

The glass transition temperature (T_g) of the tested polyimides taken as the midpoint of the change in slope of the baseline has been derived from DSC analyses (not reported) and it was 350 °C for BPDA-3F and 400 °C for 6FDA-DAD. The decomposition temperatures, as derived from the onset of each thermogravimetric curve, were in both cases larger than 400 °C.

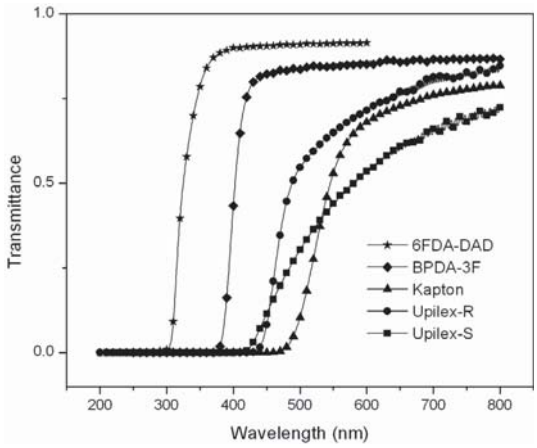

Fig. 4. UV-vis transmission spectra of 6FDA-DAD and BPDA-3F compared with the commercially available Upilex-R, Upilex-S and Kapton polyimides.

Table 1. Onset and 80% transmission wavelengths from UV-vis spectra for 6FDA-DAD, BPDA-3F and commercially available polyimides.

Polyimide	80% Transmission wavelength (nm)	UV-visible cut off wavelength (nm)
UPILEX-R	700	425
UPILEX-S	>800	425
KAPTON	800	456
6FDA-DAD	353	295
BPDA-3F	433	375

3.2 Composition and structure evolution during the ion-exchange process and thermal annealing

The structural changes of both the 6FDA-DAD and BPDA-3F polyimides during the nucleophilic attack with KOH for different times have been monitored by FT-IR spectroscopy.

As displayed in Figures 5a and 5b, for both polyimides the ring opening reaction caused by the nucleophilic attack of OH^- on the carbonyl carbon of the imide moiety is clearly evidenced by the decrease of both the signals at about 1780 and 1720 cm^{-1}, assigned to the symmetric and asymmetric stretching of the carbonyl groups of the imide ring (imide I).

The new strong components which appear for both polyimides in the range 1660−1510 cm^{-1} after KOH treatment are ascribed to the presence of amide and carboxylate groups [24]. Therefore, the kinetics of the alkaline hydrolysis reaction with polyamate formation can be followed by observing the changes in the ratio of absorption of the imide I band near 1780 cm^{-1} with the absorption of a reference band (-CF_3 stretching in the range 1180−1260 cm^{-1} for both polyimides), as a function of the KOH treatment time, as reported in Figure 6 for both

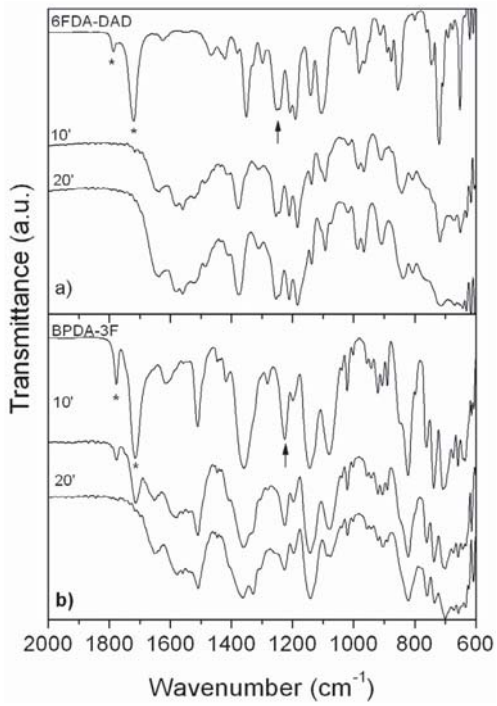

Fig. 5. ATR FT-IR spectra for polyimide films of 6FDA-DAD (a) and BPDA-3F (b) recorded after different treatment times in KOH 5M at 45 °C. The imide I spectral features are marked with an asterisk, whereas the reference band is indicated by the arrow.

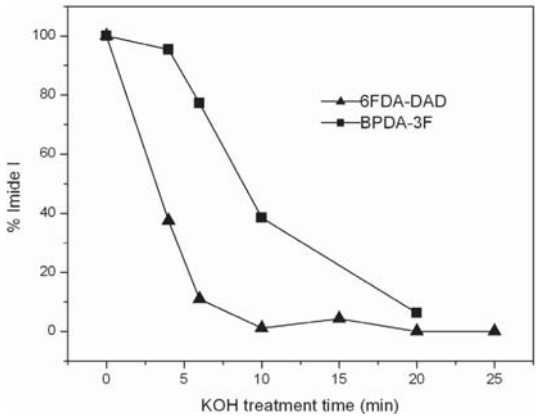

Fig. 6. Time evolution of the imide I peak intensity for both polyimides 6FDA-DAD and BPDA-3F immersed in KOH 5M at 45 °C.

polyimides. After about 20 min treatment time the whole layer probed by the IR beam is modified by hydrolysis. It is clearly evident from the plot that 6FDA-DAD undergoes a more rapid nucleophilic attack with respect to BPDA-3F. After 10 min of immersion in KOH, the imide component is completely disappeared in 6FDA-DAD, whereas in BPDA-3F about 40% of the initial imide is still present.

The different modification speed of the two types of polyimides could stem from the different reactivity of the imide carbonyl groups. In 6FDA-DAD the electron withdrawal action of the hexafluoroisopropylidene

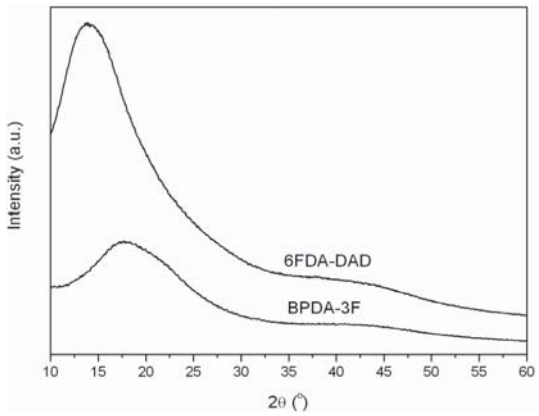

Fig. 7. XRD patterns of the 6FDA-DAD and BPDA-3F bare polyimides.

unit of the dianhydride portion promotes the reaction between the carbonyl carbon with the strong nucleophile OH^-, whereas the presence of the weak electron donating biphenyl group in BPDA-3F adversely affects the carbonyl reactivity towards the nucleophile attack. Furthermore, the different response to the KOH treatment can be correlated to a different diffusion rate of the reactant OH- through the macromolecules. As a matter of fact, it has been reported that 6FDA-DAD displays a much higher permeability than BPDA-3F [25]. This feature is correlated to the chemical structure of 6FDA-DAD, where both the presence of the bulky hexafluoropropane group -$C(CF_3)_2$- in the dianhydride portion and the presence of methyl substituents in the *ortho* position of the diamine moiety, which adversely affects the free rotation of the phenyl group around the imide –C-N- bond, hinder the molecular linearity and co-planarity, thus preventing a tight stacking of the chains. Hence, on the basis of the chemical structure, which is correlated to the permeability features, the interchain distance of 6FDA-DAD is expected to be higher than in BPDA-3F, thereby allowing a faster penetration of the nucleophile. XRD measurements have been performed to estimate the interchain distance of the bare polyimides, according to the procedure described by Kim and co-workers [26]. The XRD spectra of both the untreated polyimides are reported in Figure 7.

The amorphous scattering gives rise to a broad band, which implies a *d*-spacing distribution. From the Bragg's rule, the average *d*-spacing values can be obtained using the X-ray diffraction angle of maximum peak intensity (θ) and the X-ray radiation wavelength (1.54 Å). The calculation yields a *d*-spacing value of 4.83 Å for BPDA-3F and 6.32 Å for 6FDA-DAD. As expected, the average interchain distance in the latter polyimide is higher, thereby confirming that the higher hydrolysis rate observed for 6FDA-DAD with respect to BPDA-3F can derive from the higher diffusion rate of KOH through the 6FDA-DAD polyimide.

FT-IR spectra recorded after annealing of the ion-exchanged samples at 200 °C and 300 °C are reported in Figure 8 for both polyimides. The recovery of the pristine polyimide structure is almost complete upon annealing

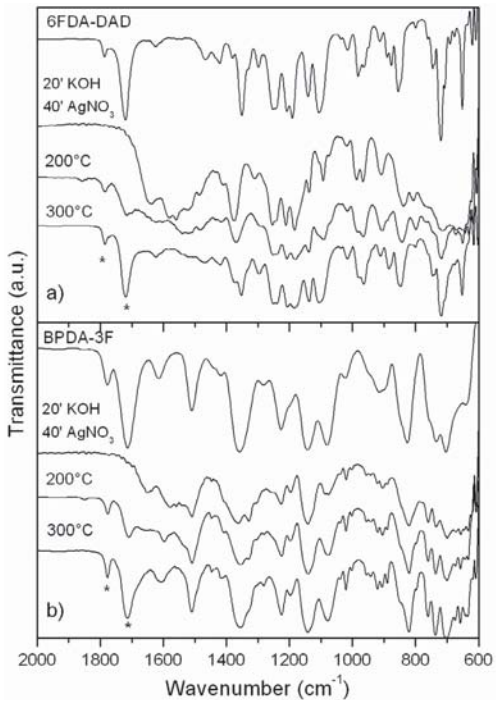

Fig. 8. ATR FT-IR spectra of 6FDA-DAD (a) and BPDA-3F (b) recorded after treatment in KOH for 20 min followed by ion-exchange in $AgNO_3$ solution and annealed at 200 and 300 °C. The imide I spectral features are marked with an asterisk.

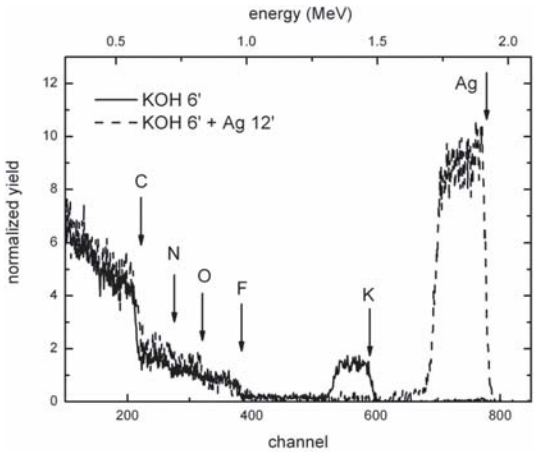

Fig. 9. Example of RBS spectra of the polyimide BPDA-3F treated in KOH (solid line) and ion-exchanged in $AgNO_3$ solution (dashed line). The details on the treatment times are reported.

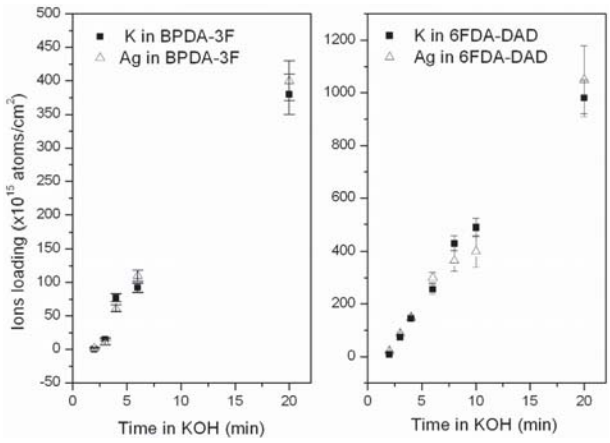

Fig. 10. Loadings of potassium and silver atoms in BPDA-3F (left) and 6FDA-DAD (right) as a function of the treatment time in KOH.

at 300 °C for both polyimides, as evidenced by the reappearance of the typical imide I spectral features at 1780 and 1720 cm^{-1}.

RBS analysis was performed in order to obtain information about the process of K penetration into the polyimide matrix and the ion exchange between K^+ and Ag^+ ions. Just after KOH treatment, the K distribution results in a flat profile, with a very sharp interface between the surface modified layer and the underlying polyimide. In Figure 9 the RBS spectra of BPDA-3F after treatment in KOH and after ion-exchange in $AgNO_3$ solution are reported as an example. The arrows indicate the channel corresponding to the energy of He particles backscattered by the different species located at the surface of the film. The total amount of loaded K and Ag atoms as a function of the treatment time in KOH is given in the plots of Figure 10 for both polyimides.

A strong correlation between the degree of alkaline hydrolysis as evidenced by FTIR analyses and the amount of loaded silver ions is evident: for the same treatment time in KOH the polyimide 6FDA-DAD allows the incorporation of a much greater amount of silver with respect to BPDA-3F, as a result of both the higher reactivity and the higher permeability towards the OH^- nucleophile.

A homogeneous in-depth concentration of potassium of about 3.7% at. in 6FDA-DAD and 3.0% at. in BPDA-3F has been detected in the modified surface layer. It is worth to note that by taking into account the chemical formula of each polyimide repeating unit ($C_{29}H_{18}O_4N_2F_6$ for 6FDA-DAD and $C_{36}H_{19}O_4N_2F_3$ for BPDA-3F), the measured atomic percentage demonstrates that the ratio of K ions:polymer repeating unit is about 2:1, thereby proving that the reaction of the polyimide with KOH is complete and both the imide rings present in each repeating unit are converted in carboxylate anions coordinated with K ions (see Fig. 3). The K penetration depth has been obtained from the simulation with the RUMP code of each recorded RBS spectrum and the results are reported in Figure 11. The linear trend exhibited by the samples as a function of the treatment time for both the polyimides indicates that the chemical reaction between KOH and the polyimide, regulating the K penetration, is a first order process within the KOH treatment time interval used in these experiments. Moreover, the K penetration rate, as obtained by RBS measurements, is higher in 6FDA-DAD (0.20 ± 0.02 μm/min) than in BPDA-3F (0.12 ± 0.02 μm/min), thus confirming the results obtained from FT-IR analyses.

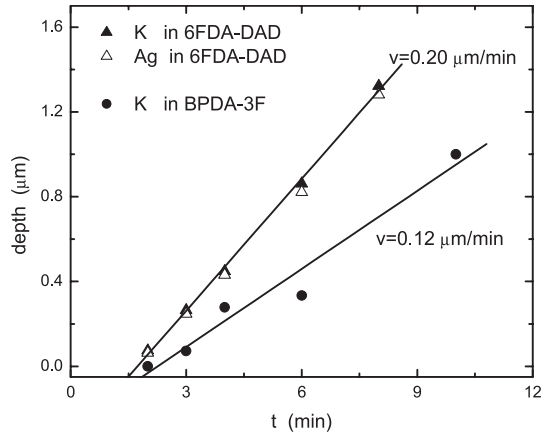

Fig. 11. Penetration depth for K vs. time treatment in KOH. For 6FDA-DAD the penetration depth of Ag is also reported, in order to highlight the complete exchange between K^+ and Ag^+ ions. The linear fits allow to estimate the speed of the K penetration process.

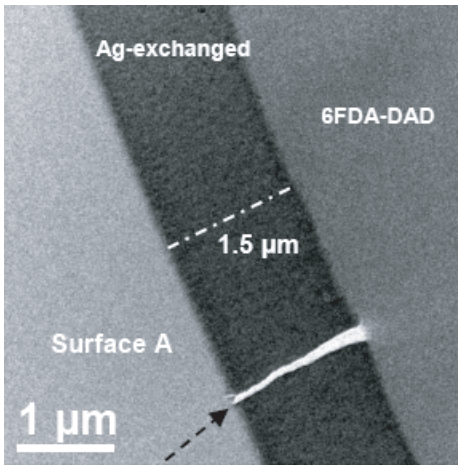

Fig. 12. Cross sectional TEM image of 6FDA-DAD treated for 10 min in KOH, for 20 min in $AgNO_3$ solution and annealed at 300 °C in reducing atmosphere, showing the thickness of the modified layer. The arrow indicates a crack in the modified layer.

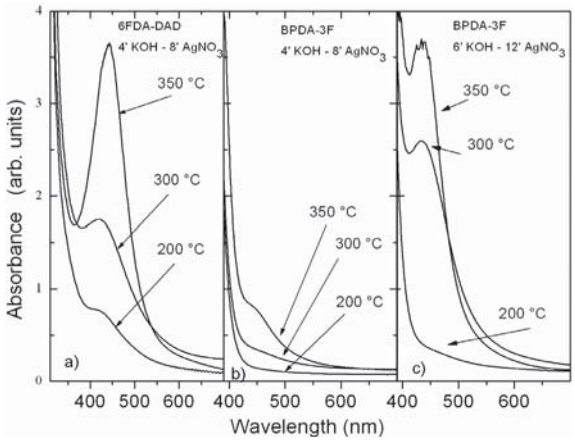

Fig. 13. Absorption spectra of 6FDA-DAD (a) and BPDA-3F (b) treated for 4 min in KOH, for 8 min in $AgNO_3$ solution and annealed at 200, 300 and 350 °C in reducing atmosphere. The spectra of BPDA-3F treated for 6 min in KOH, 12 min in $AgNO_3$ are also reported in (c).

As far as the process of Ag doping is concerned, RBS analysis detected a complete emptying of K, as a result of the treatment in $AgNO_3$ solution and a 1:1 substitution of K^+ by Ag^+ within the experimental errors in all the samples, as can be observed from the data of Figure 10. As a matter of fact, Ag exhibits a flat concentration profile (3.7% at. in 6FDA-DAD and 3.0% at. in BPDA-3F) and its penetration depth is determined by the thickness of the KOH modified layer, as demonstrated by the data relative to 6FDA-DAD reported in Figure 11. On the other hand, no silver was detected in polyimide thin films which did not undergo any pre-treatment in KOH before the immersion in $AgNO_3$ aqueous solution, thus indicating that the step of potassium polyamate salt formation is needed to achieve the Ag doping of the polyimide.

The concentration profile of Ag was also measured in the samples after thermal treatments at 200, 300 and 350 °C in reducing atmosphere. The influence of the annealing temperature on the Ag in-depth distribution is negligible, thus indicating that silver reduction and clusters formation and growth occur uniformly within the depth without significant migration phenomena. TEM analyses performed on the sample 6FDA-DAD treated for 10 min in KOH, 20 min in $AgNO_3$ and annealed at 300 °C in reducing atmosphere confirmed the experimental RBS results as regarding the penetration depth of Ag (estimated in 1.6 μm for this sample), as clearly observed in the micrograph reported in Figure 12, and the homogeneity of the silver clusters distribution, as evidenced in the micrographs of Figure 16.

3.3 Silver clusters characterization

Absorption spectra from samples treated for 4 minutes in KOH and for 8 minutes in $AgNO_3$ solution are reported in Figures 13a and 13b for annealing temperatures of 200, 300 and 350 °C. 6FDA-DAD treated at 200 °C exhibits a faint shoulder at about 420 nm, which grows up at 300 °C and becomes a well defined peak at 440 nm after annealing at 350 °C. On the other hand, the absorption spectrum at 200 °C of BPDA-3F does not exhibit any SPR feature, and at 300 °C a faint and broad band appears at about 440 nm, whose intensity slightly increases at 350 °C. The concentration of silver atoms in the samples is about the same, as revealed by RBS measurements. However, the comparison between the spectra of the two polyimides is not meaningful in this case, since the absorption peak intensity is correlated to the total amount of silver clusters present in the whole layer. Moreover, the cut-off wavelength of the polyimides, as reported in Table 1, must be taken into account. In the range 420−440 nm the transmission percentage varies from 75 to 82% in the case of BPDA-3F, whereas the transmittance of 6FDA-DAD polyimide is about constant at 90%.

On the basis of the total silver ions loading reported in Figure 10, a more significant comparison should be derived from the spectra of 6FDA-DAD treated for 4 min in KOH, 8 min in $AgNO_3$ and those of BPDA-3F treated for 6 min in KOH, 12 min in $AgNO_3$. The latter ones are reported in Figure 13c. After the treatment at 200 °C the BPDA-3F sample displays only a faint increase in the absorption baseline, but the SPR peak features are still absent. After the treatment at 300 °C, the same sample shows a very intense SPR peak at about 433 nm. The SPR absorption intensity is almost the same for the samples treated at 350 °C. Many factors contribute to the process of formation and growth of the silver clusters, so that in order to analyze the optical absorption spectra it is important to summarize the different steps which are involved during the thermal treatment in reducing atmosphere.

Ikeda and co-workers [19] have already pictured the re-imidization process in the case of Cu(II) ion doping in PMDA-ODA polyimide. Metal reduction is attained by accepting electrons from molecular hydrogen, then the carboxylate anions are immediately protonated and converted in polyamic acid groups. The temperature is high enough (200 °C) to allow the de-hydration and condensation reaction of carboxylic groups to form imide rings. However, the stability of the metal-polyamate complex can play an important role on the overall reduction/re-imidization process rate.

One of the most stable forms of the silver (I) complexes is the linear one, thus it can be predicted that in the present case the carboxylate ligand has the unidentate form and it behaves as one-electron donor. In this configuration, the stability of the silver (I) complex depends on the electron-donating ability of the carboxylate oxygen atom. In the 6FDA-DAD derived polyamate, the electron withdrawing hexafluoro isopropylidene moiety is expected to lower the carboxylate donating capability, thereby producing a less stable silver (I) complex than in the case of BPDA-3F polyamate.

On the basis of these considerations, a correlation between the SPR peak intensity and the silver (I) reduction process in the different polyimides annealed at 200 °C can be found.

At 200 °C the reduction of silver ions is not effective in the BPDA-3F sample as in 6FDA-DAD, owing to the higher silver (I) complex stability in the former system. Hence, the SPR peak features are not visible in the BPDA-3F sample.

At 300 °C the re-imidization of both polyimides and the consequent reduction to metallic silver is complete. The SPR peak intensity increases accordingly in both samples. The aforementioned lower transparency in the wavelength range of interest of the bare BPDA-3F polyimide accounts for the higher absorption edge observed in the spectra of the BPDA-3F derived samples. Although nanoclusters average diameter can be derived using the full width half maximum (FWHM) of the SPR peak, according to the literature [27], the contribution of the background arising from the polyimide matrix can not be easily removed without introducing some artefacts, such as modification of peak position and peak shape, thus leading to misinterpretation of data.

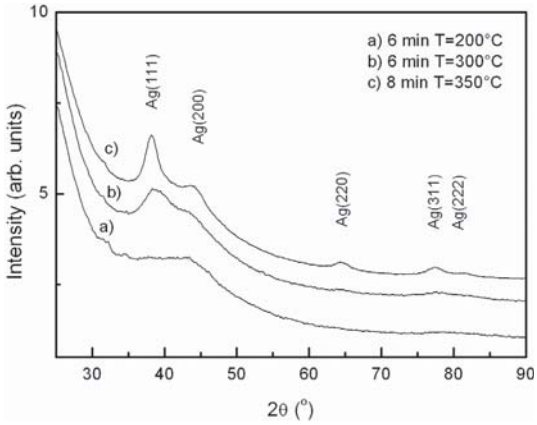

Fig. 14. XRD spectra of BPDA-3F treated for 6 min in KOH, 12 min in $AgNO_3$ and annealed at 200 °C and 300 °C in reducing atmosphere. The spectrum of the sample treated for 8 min in KOH, 16 min in $AgNO_3$ and annealed at 350 °C is also reported.

Therefore, the information on the nanocrystals size and size distribution must be inferred from X-ray diffraction and TEM analyses.

The clusters crystal structure was investigated by X-ray diffraction and the results for samples of BPDA-3F treated for 6 min in KOH, 12 min in $AgNO_3$ and annealed at 200 and 300 °C are presented in Figure 14 (curves a and b). The spectrum of the sample treated for 8 min in KOH, 16 min in $AgNO_3$ and annealed at 350 °C is also reported (curve c).

At 300 °C the two main peaks of fcc silver can be observed, thereby proving that in this temperature regime precipitation of metallic silver already occurred. In the spectrum of the sample annealed at 350 °C the peaks are well defined and the intensity grows up as a result of complete silver reduction and crystal growth.

In order to compare the silver crystals growth in the two polyimides, the XRD spectra of 6FDA-DAD and BPDA-3F treated for the same time in KOH and $AgNO_3$ and annealed at 300 °C have been collected and are reported in Figure 15. Using the well-known Scherrer's formula, the average crystallites size has been calculated by the full width half maximum (FWHM) of the Ag (111) diffraction peak, for both 6FDA-DAD and BPDA-3F treated for different times and annealed at 300 °C. The results are reported in the inset of Figure 15 and they evidence that almost comparable clusters dimensions have been obtained in both polyimides. The clusters size ranges from 2 up to 3.5 nm and it is negligibly affected by the treatment time in KOH.

Further investigations on the nanocomposite structure have been performed using TEM analyses. Figures 12 and 16 report a series of cross sectional bright field micrographs of 6FDA-DAD, treated for 10 min in KOH, for 20 min in $AgNO_3$ and then annealed at 300 °C. Along the doped layer, whose mean thickness is 1.5 μm in agreement

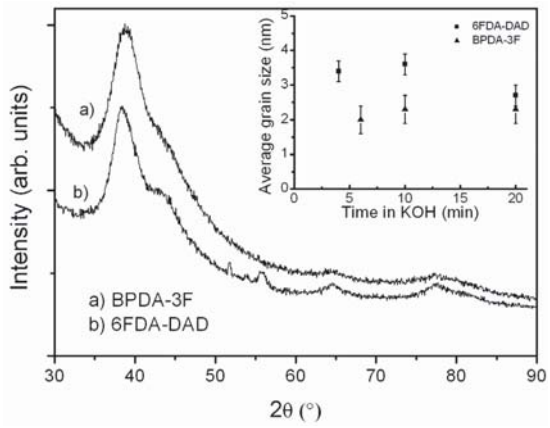

Fig. 15. XRD spectra of 6FDA-DAD and BPDA-3F treated for 20 min in KOH, 40 min in $AgNO_3$ and annealed at 300 °C in reducing atmosphere. In the inset, the average grain size of silver crystals as derived from the Scherrer's formula is reported for both modified polyimides annealed at 300 °C as a function of the treatment time in KOH.

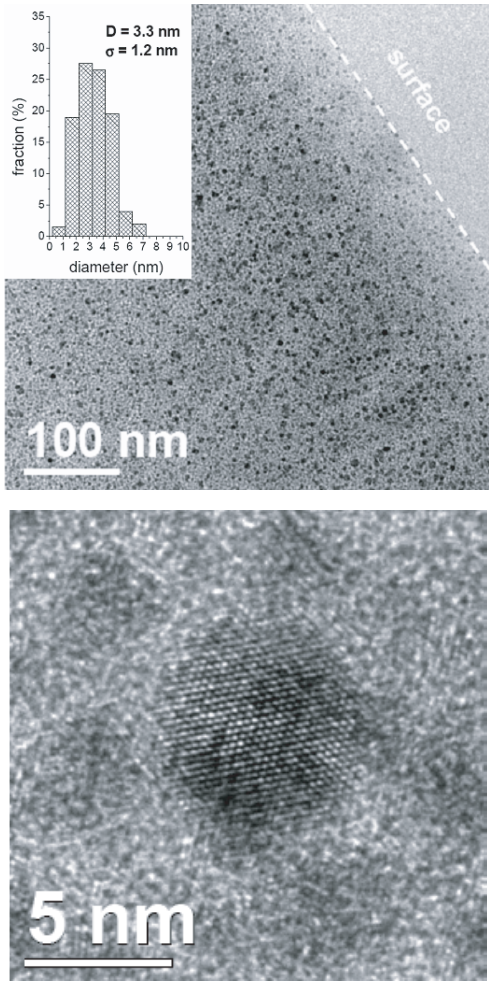

Fig. 16. Cross sectional TEM images at different magnifications of 6FDA-DAD treated for 10 min in KOH, for 20 min in $AgNO_3$ solution and annealed at 300 °C in reducing atmosphere. In the inset of the upper image, the size histogram is reported.

with RBS data, a uniform distribution of spherical silver clusters can be observed. The mean size was evaluated to be $\langle D \rangle = 3.3$ nm with standard deviation $\sigma = 1.2$ nm, as shown by the histogram of Figure 16.

4 Conclusions

The formation of silver nanoparticles in transparent fluorinated polyimides, as a consequence of K-assisted Ag doping and thermal reduction in hydrogen atmosphere, has been studied using different microanalytical, microstructural and optical techniques. The first stage of the process, leading to the formation of the potassium polyamate salt, and the following K^+-Ag^+ ion-exchange process have been correlated to the starting polyimide chemical structure. RBS analysis evidenced that the K penetration depth is a linear function of the treatment time in KOH, thereby proving that the chemical reaction between the nucleophile and the polyimide is in both cases a first order process. Moreover, the K penetration rate depends on the polyimide structure: both the chemical nature of the substituents along the polymeric chain and the network permeability to aqueous solution are considered to affect the K penetration rate. XRD measurements have been used to estimate the intersegmental distance (d-spacing) in both the original polyimides and the results evidenced a loosened chain packing in 6FDA-DAD with respect to BPDA-3F, thus proving that a faster permeation of the KOH solution through the 6FDA-DAD matrix can effectively occur.

The ion-exchange step in $AgNO_3$ solutions affords complete substitution of K by Ag ions in both polyimides, within the treatment times used in these experiments. The Ag nanocrystals precipitation in reducing atmosphere has been correlated to the silver reduction process, which in turns is related to the silver (I) polyamate complex stability in the two different polyimides. The subsequent step of clusters growth as a function of the annealing temperature has been investigated by XRD and TEM analyses. Similar clusters dimensions have been estimated in the different polyimides, ranging from 2 to 3.5 nm. The effective application of such nanocomposites for optical gas sensors is currently under investigation.

This research was financially supported by the Fifth Commission of Istituto Nazionale di Fisica Nucleare (ASTHICO project) and by Micropolys FIRB 2003 project.

References

1. F. Gonella, P. Mazzoldi, in *Handbook of Nanostructured Materials and Nanotechnology*, edited by H. Nalwa (Academic, San Diego, 2000), Vol. 4, Chap. 2
2. A.N. Shipway, Chem. Phys. Chem. **1**, 18 (2000)
3. U. Kreibig, M. Vollmer, *Optical Properties of Metal Clusters* (Springer, Berlin, 1995)
4. P. Mulvaney, Langmuir **12**, 788 (1996)
5. G. Chumanov, K. Sokolov, B.W. Gregory, T.M. Cotton, J. Phys. Chem. **99**, 9466 (1995)

6. J. Matsui, K. Akamatsu, S. Nishiguchi, D. Miyoshi, H. Nawafune, K. Tamaki, N. Sugimoto, Anal. Chem. **76**, 1310 (2004)
7. C. de Julián Fernández, M.G. Manera, J. Spadavecchia, G. Maggioni, A. Quaranta, G. Mattei, M. Bazzan, E. Cattaruzza, M. Bonafini, E. Negro, A. Vomiero, S. Carturan, C. Scian, G. Della Mea, R. Rella, L. Vasanelli, P. Mazzoldi, Sens. Actuators B **111-112**, 225 (2005)
8. Y. Dirix, C. Bastiaansen, W. Caseri, P. Smith, J. Mater. Sci. **34**, 3859 (1999)
9. H. Biederman, Vacuum **37**, 367 (1987)
10. K. Akamatsu, T. Kawamura, H. Nabika, S. Deki, T. Strunskus, F. Faupel, J. Mater. Chem. **12**, 3610 (2002)
11. R.J. Angelo, U.S. Patent 3,073,785 (1959)
12. M.W. Wllison, L.T. Taylor, Chem. Mater. **6**, 990 (1994)
13. R.E. Southward, D.W. Thompson, Chem. Mater. **16**, 1277 (2004)
14. S. Yoda, A. Hasegawa, H. Suda, Y. Uchimaru, K. Haraya, T. Tsuji, K. Otake, Chem. Mater. **16**, 2363 (2004)
15. A.L. Stepanov, Tech. Phys. **49**, 143 (2004)
16. G. Maggioni, A. Vomiero, S. Carturan, C. Scian, G. Mattei, M. Bazzan, C. de Juliàn Fernandez, P. Mazzoldi, A. Quaranta, G. Della Mea, Appl. Phys. Lett. **85**, 5712 (2004)
17. K. Akamatsu, S. Ikeda, H. Nawafune, S. Deki, Chem. Mater. **15**, 2488 (2003)
18. K. Akamatsu, Eur. Phys. J. D **24**, 377 (2003)
19. S. Ikeda, K. Akamatsu, H. Nawafune, T. Nishino, S. Deki, J. Phys. Chem. B **108**, 15599 (2004)
20. Y. Li, Q. Lu, X. Qian, Z. Zhu, J. Yin, Appl. Surf. Sci. **233**, 299 (2004)
21. S. Sasaki, S. Nishi, in *Polyimides: fundamentals and applications*, edited by Ghosh, Mittal (Marcel Dekker Inc., New York, 1996), p. 71
22. W.B. Alston, R.F. Gratz, US Patent 4,885,116 (1989)
23. L.R. Doolittle, Nucl. Instrum. Meth. B **9**, 334 (1985)
24. R.M. Silverstein, G.C. Bassler, T.C. Morrill, in *Spectrometric Indentification of Organic Compounds* (J. Wiley & Sons, New York, 1981), p. 116
25. A.Y. Alentiev, K.A. Loza, Y.P. Yampolskii, J. Membr. Sci. **167**, 91 (2000)
26. T.H. Kim, W.J. Koros, G.R. Husk, K.C. O'Brien, J. Membr. Sci. **37**, 45 (1988)
27. G.W. Arnold, J. Appl. Phys. **46**, 4466 (1975)